Inside New Materials: An Experimental Numerical Approach for the Structural Elucidation of Nanoporous Cross-Linked Polymers

ARTICLE *in* THE JOURNAL OF PHYSICAL CHEMISTRY B · OCTOBER 2012

Impact Factor: 3.3 · DOI: 10.1021/jp307978e · Source: PubMed

7 AUTHORS, INCLUDING:

Vincenza Crupi
Università degli Studi di Messina
162 PUBLICATIONS **1,624** CITATIONS
SEE PROFILE

Andrea Mele
Politecnico di Milano
208 PUBLICATIONS **2,716** CITATIONS
SEE PROFILE

Barbara Rossi
Elettra, Sincrotrone Trieste S.C.p.A.
63 PUBLICATIONS **430** CITATIONS
SEE PROFILE

Francesco Trotta
Università degli Studi di Torino
150 PUBLICATIONS **2,501** CITATIONS
SEE PROFILE

THE JOURNAL OF PHYSICAL CHEMISTRY B

Article

pubs.acs.org/JPCB

Inside New Materials: An Experimental Numerical Approach for the Structural Elucidation of Nanoporous Cross-Linked Polymers

Francesca Castiglione,[†] Vincenza Crupi,[‡] Domenico Majolino,[‡] Andrea Mele,[†,§] Barbara Rossi,*[,∥,⊥] Francesco Trotta,[#] and Valentina Venuti[‡]

[†]Department of Chemistry, Materials and Chemical Engineering "G. Natta", Politecnico di Milano, Piazza L. Da Vinci, 32 20133 Milano, Italy

[‡]Dipartimento di Fisica e di Scienze della Terra, Università di Messina, Viale Ferdinando Stagno D'Alcontres 31, 98166 Messina, Italy

[§]CNR- Istituto di Chimica del Riconoscimento Molecolare, via L. Mancinelli 7, 20131 Milano, Italy

[∥]Dipartimento di Informatica, Università di Verona, Strada le Grazie 15, 37134 Verona, Italy

[⊥]Dipartimento di Fisica, Università di Trento, via Sommarive 14, 38123 Povo, Trento, Italy

[#]Dipartimento di Chimica, Università di Torino, Via P. Giuria 7, 10125 Torino, Italy

Supporting Information

ABSTRACT: An integrated experimental-numerical approach, based on vibrational spectroscopy techniques and quantum chemical computation methods, has been here implemented and tested on a new class of cyclodextrin-based cross-linked polymers, namely, cyclodextrins nanosponges. By the simultaneous quantitative analysis of FTIR-ATR and Raman spectra in the frequency domains between 1650−1800 and 3000−3700 cm^{-1}, we individuated reliable physical descriptors directly connected to the cross-linking degree of the polymeric matrices. The comparison between the experimental data and the results of the quantum chemical simulations provided structural information on the involvement of the cyclodextrin chemical groups during the polymerization process. This proposed experimental numerical approach appears to be of general application for the investigation of amorphous polymeric matrices of interest for technological application, for which the use of other experimental techniques is seriously hampered by the low or absent level of crystallinity.

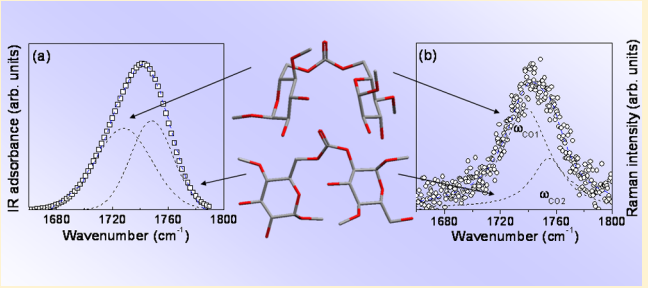

INTRODUCTION

Cyclodextins (CDs) are cyclic oligomers of amilose with consolidated and well-assessed characteristics of host molecules for supramolecular inclusion complexes.[1−7] CDs are torus-shaped molecules with external hydrophilic surface and an inner, lipophilic cavity. The most common CDs are made of six, seven, or eight glucopyranose units, and they are referred to as α-, β-, or γ-CD. Hydrophobic molecules, or molecules containing one or more apolar groups, can be included in the CD's cavity by hydrophobic interactions, giving rise to stable, noncovalent inclusion complexes.[8−10] These host−guest complexes find several applications, mainly in the pharmaceutical field, such as water solubility enhancement, controlled release, and stabilization of active pharmaceutical ingredients.[2−4] Moreover, the presence of several OH groups on CD makes these molecules appealing monomers for polymerization.[7,11] Recently, the easy preparation of cross-linked polymers by reaction of CD with suitable activated derivatives of carboxylic acids has been proposed.[12] The corresponding materials are referred to as CD nanosponges (CDNSs).[12] CDNSs are insoluble in water and in most common organic solvents, but some classes of CDNSs may undergo swelling in the presence of aqueous solutions. The main feature of these polymeric matrices is the simultaneous presence of lyphophilic cavities and hydrophilic channels, which can be used to encapsulate, carry, and release a great variety of substances. Moreover, the surface charge density, the porosity, and the pore sizes of CDNS can be properly controlled during the synthesis to tune the entrapment/release properties of these matrices for specific technological applications. For example, some types of nanosponges have been successfully used for the removal of organic impurities from water[13−16] and as efficient flame-retardant systems.[17,18]

Recently, many studies have been conducted on the drug delivery capabilities of these polymeric matrices, showing that CDNS can efficiently encapsulate, carry, and gradually release over extended times different types of lipophilic and hydrophilic drug molecules, increasing their bioavailability at the target site.[19−24]

Received: August 10, 2012
Revised: October 12, 2012
Published: October 16, 2012

As previously reported, the thorough physico-chemical and structural characterization of these materials is a challenging task, and several spectroscopic methods are being used.

For example, we recently studied β-CDNS obtained from pyromellitic dianhydride (PMA) as cross-linking agent at different β-CD/PMA molar ratios.[25−27] Raman spectroscopy on both dry and water-treated samples was successfully used to spot on the cross-linking degree by the inspection of the low-frequency dynamics, sensitive to stiffness of the system.[25,26] The swelling process of CDNS was investigated by the analysis of the O−H and C−H groups vibrational modes.[25] Powder X-ray diffraction data indicated low crystallinity of CDNS, whereas high-resolution magic-angle spinning nuclear magnetic resonance (HRMAS-NMR) measurements on hydrated samples gave clues of "free" and "bound" water molecules in the polymeric gel with different diffusion coefficients.[25] Finally,[27] Fourier transform infrared spectroscopy in attenuated total reflectance geometry (FTIR-ATR) allowed us to elucidate the effect of temperature and cross-linking degree on a network of hydrogen bonds contributing to the high-frequency vibrational dynamics of the nanosponge.

The present study reports on the results of a multitechniques investigation carried out on β-CDNS obtained by reacting β-CD with carbonyldiimidazole (CDI) at four different β-CD/CDI molar ratios.[15] CDI acts as synthetic equivalent to phosgene, inserting a carbonyl group between two free OH groups of CD with the formation of carbonate ester (Figure 1).

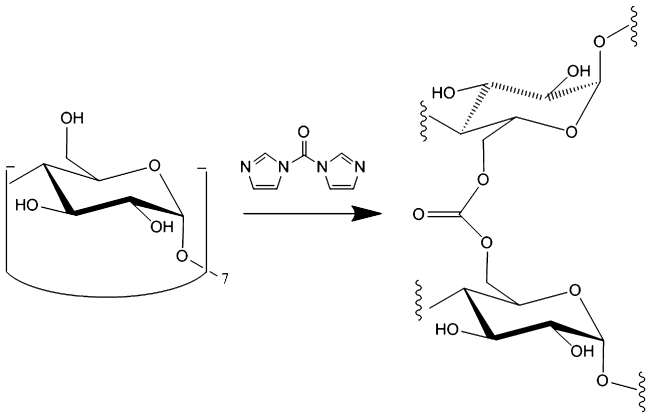

Figure 1. Scheme of formation of carbonate bridge between two adjacent cyclodextrins.

The corresponding nanosponges used in the present work were synthesized by using four different β-CD/CDI molar ratios,[28] with the main purpose of clarifying the role played by such parameter on the cross-linking density of the final polymeric network. The detailed analysis of the spectral properties of the vibrational band of carbonyl groups observed in the IR and Raman spectrum of CDI-nanosponges at different β-CD/CDI molar ratios is carried out by using best-fitting and deconvolution procedures. The spectral analysis is supported by ab initio calculations to compute the vibrational frequency of C═O groups in different molecular environments. In a parallel way, information on the reactive sites of CD and possible regioisomers distribution in the formation of the carbonate junction among different CD units are collected and analyzed by deconvolution of the O−H stretching region.

EXPERIMENTAL SECTION

A. Synthesis of β-CDCDI Nanosponges. To obtain β-CDCDI1n nanosponges, we conducted the reactions of polymerization between β-CD and the cross-linking agent CDI at molecular ratios of 1:n (with n = 2, 3, 5, 8), dissolving β-CD in anhydrous dimethylformamide (DMF). Once the required molar amount of cross-linking agent CDI was added, the mixture was allowed to react for 4 h at T = 100 °C. The reaction mixture first became more viscous during the time, and a monolithic block was obtained once the reaction is over. The eventually unreacted CDI was completely decomposed with water at room temperature, leading imidazole and evolving CO_2 as by products. Imidazole is soluble in water, and it is removed by prolonged washing. The absence of CO_2 is indirect evidence of the completeness of the reaction. Once the reaction was over, a great excess of water was added and the solid was recovered by filtration under vacuum, washed with ethanol, and then Sohxlet extracted with ethanol for 10 h.

B. FTIR-ATR Measurements. FTIR−ATR absorption measurements were performed on dried samples in the 600−4000 cm^{-1} wavenumber range in the temperature range extending from 250 to 320 K. Spectra were recorded using a Bomem DA8 Fourier transform spectrometer, operating with a Globar source, in combination with a KBr beamsplitter, a DTGS/KBr detector. The powders were contained in Golden Gate diamond ATR system, just based on the ATR technique. An ATR setup exhibits various advantages with respect to an ordinary absorption setup. It is nondestructive, it requires only micrograms of sample, and it is at the origin of spectra displaying a very good signal-to-noise ratio, being, in particular, easy to avoid saturation of bands. In addition, a chemical analysis can be performed directly on ATR spectra, avoiding implementation of elaborated calculations of optical constants. The spectra were recorded in dry atmosphere to avoid dirty contributions with a resolution of 2 cm^{-1}, automatically adding 100 repetitive scans to obtain a good signal-to-noise ratio and high reproducibility. All IR spectra were normalized for taking into account the effective number of absorbers. No mathematical correction (e.g., smoothing) was done, and spectroscopic manipulation such as baseline adjustment and normalization were performed using the Spectracalc software package GRAMS (Galactic Industries, Salem, NH). For both the C═O and the O−H stretching region, second-derivative computations, not reported here, have been used for evaluating the wavenumbers of the maxima of the different sub-bands. The presence, in the experimental spectra, of, respectively, two sub-bands for the C═O stretching region and five sub-bands for the O−H stretching mode with the assigned centerfrequencies was suggested by, respectively, the two and five minima observed in the second-derivative profiles approximately corresponding to the maxima of each band component. Band decomposition was then undertaken, by multiple curve fitting into Voigt profiles applied to the experimental spectra based on these wavenumber values. We used the routine provided in the PeakFit 4.0 software package. The statistical parameters defined in the software manual were used as a guide to "best-fit" iteration until converging solution was reached. Although the spectral decompostion procedures have no unique solution, we remark that the one we adopted here uses the minimum number of parameters, and, at the same time, it furnishes extremely good fits to the data. In both cases, the "best-fit" is, in fact, characterized by $r^2 \approx 0.9999$ for all investigated systems.

dx.doi.org/10.1021/jp307978e | J. Phys. Chem. B 2012, 116, 13133−13140

C. Raman Measurements. Raman spectra were recorded on dried samples deposited on a glass slide in air at room temperature by means of a microprobe setup (Horiba-Jobin-Yvon, LabRam Aramis) consisting of a He−Ne laser, a narrow-band notch filter, a 46 cm focal length spectrograph using a 1800 grooves/mm grating, and a charge-coupled device (CCD) detector. Exciting radiation at 632.8 nm was focused onto the sample surface with a spot size of ∼1 μm^2 through a 100× objective with NA = 0.9. To avoid unwanted laser-induced transformations, we used neutral filters of different optical densities whenever necessary. Spectra were collected in the wavenumber range 100−3700 cm^{-1}. The resolution was ∼0.35 cm^{-1}/pixel.

D. Computational Methods. The formation of carbonate ester between two cyclodextrin units was mimicked by using the low-molecular-weight analogue methyl-α-D-4-*O*-methylglucopyranoside. Each glucosides has three OH groups available for reaction with CDI: OH(2), OH(3), and OH(6). The formation of the dimeric carbonate thus gives rise to six possible regioisomers, accounting for the combinations of primary and secondary OH groups of each unit (Structures **1**−**6** in Figure 2). Each carbonate was built from scratch by using

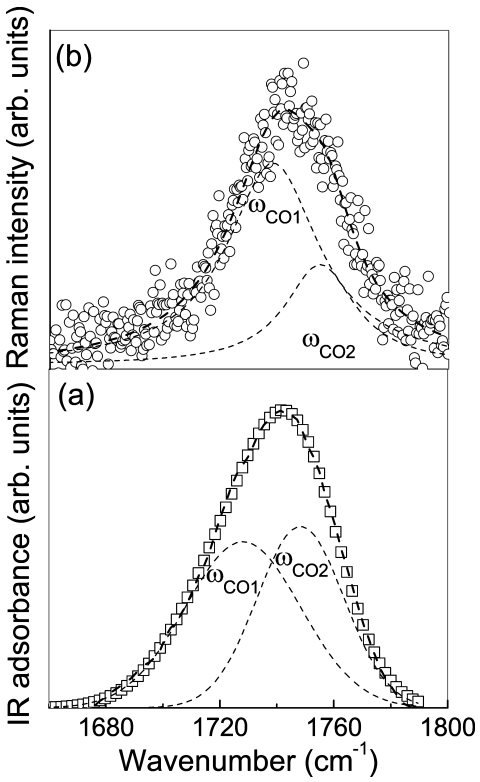

Figure 2. Experimental FTIR-ATR (a) and Raman (b) spectra for β-CDCDI15 nanosponge in the 1600−1800 cm^{-1} wavenumber range at room temperature together with the best-fit (continuous line) and the deconvolution components (dashed lines).

PCMODEL 8.0 package (Serena Software, Bloomington, IN) and allowed to relax fully in MMX force field.[29] A full conformational analysis was carried out by varying the torsion angles about the C−O bonds on both sides of the carbonate functional group in steps of 5° (subroutine Dihedral Driver of the PCMODEL 8.0 program suite). The MMX energy-minimized geometries were, in turn, used as starting structures for ab initio quantum chemical computations carried out with the GAUSSIAN 03 program suite[30] using unrestricted density functional theory (DFT).[31] The nonlocal B3LYP functional hybrid method was employed.[32] The standard 6-31G basis set[33] was used for the geometry optimization and vibrational energy analysis. For the plot of the theoretical infrared and Raman spectra, a Lorentzian line shape with a line width of 4 cm^{-1} was used; computed IR intensities and Raman activities are expressed in arbitrary units.

RESULTS AND DISCUSSION

Figure 2a,b shows, as an example, the FTIR-ATR and Raman spectra in the wavenumber range 1650−1800 cm^{-1} at room temperature for a sample of β-CDCDI15. (For nomenclature, see the Experimental Section.) A characteristic vibrational band centered at ∼1743 cm^{-1} in both IR and Raman spectrum can be observed in this specific spectral region for all samples of CDI-nanosponges investigated. This band is assigned to the stretching vibration of carbonyl C═O group of the polymeric network. It is directly connected to the population of the C═O functional groups, in turn related to the cross-linking degree of the system. The high quality of the vibrational spectra of Figure 2 makes their quantitative analysis feasible by using the second derivative computation and curve fitting procedure, which allow the deconvolution of the band observed between 1650 and 1800 cm^{-1} into the individual spectral components. However, the C═O stretching vibration is partially overlapped in both IR and Raman spectra to the band at ∼1640 cm^{-1} assigned to the δ-HOH bending of water molecules tightly bound to the β-CD units.[34] To overcome this problem, we carried out the simultaneous fit of the whole spectrum between 1500 and 1800 cm^{-1}, with all of the fitting parameters left free to vary upon iteration until convergence. Then, the contribution arising from the mode at ∼1640 cm^{-1} was subtracted from the experimental data, thus providing a more reliable fit of the C═O stretching vibration, in both FTIR-ATR and Raman spectrum. (See Figure 2.) In this way, two sub-bands for the C═O stretching band were extracted, that is, ω_{CO1} falling at ∼1730 cm^{-1} in IR and at ∼1740 cm^{-1} in Raman spectrum and ω_{CO2} found at ∼1750 cm^{-1} in IR and at ∼1760 cm^{-1} in Raman spectrum.

The slight frequency difference found for the same sub-bands, that is, ω_{CO1} and ω_{CO2}, on passing from the IR to the Raman spectrum is likely to derive from the different mathematical functions (Voigt functions for IR and Lorentzian peaks for Raman profile, respectively) used for the deconvolution of the experimental bands.

These components indicate that the carbonyl group experiences at least two different molecular environments due to the presence of regioisomeric carbonate ester formation. In other words, the carbonate group can be formed starting from OH(2), OH(3), and OH(6) of each glucose unit (standard numbering of glucose atoms). In theory, six different carbonates can be formed, accounting for the possible combinations of the OH groups able to react with CDI, as described above. Figure 3 shows the minimized structures of the six regioisomeric carbonates obtained from methyl-α-D-4-*O*-methylglucoside using a simple model mimicking the glucose connectivity in cyclodextrins.

The theoretical IR and Raman spectra were computed for all the minimized structures of Figure 3. The interesting spectral region (1650−1800 cm^{-1}) was then compared to the experimental IR and Raman spectra in the same region. This type of vibrational analysis,[35] based on the experimental-

dx.doi.org/10.1021/jp307978e | J. Phys. Chem. B 2012, 116, 13133−13140

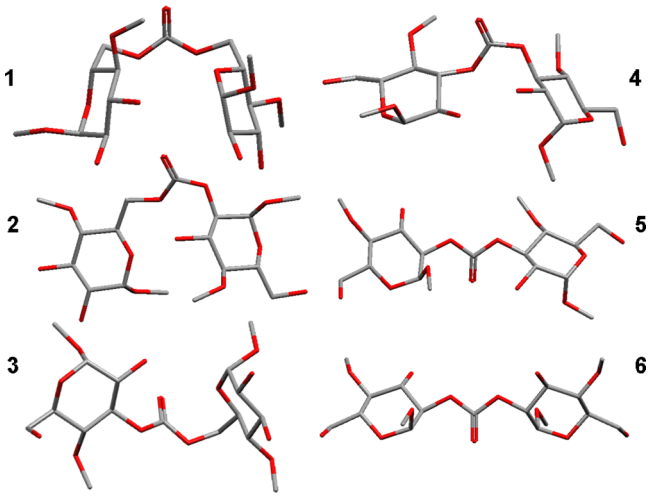

Figure 3. DFT-minimized structures of the six possible regioisomeric carbonates of model methyl-α-D-4-*O*-methylglucoside.

numerical approach, gave the results summarized in Figure 4, where the theoretical IR (left) and Raman (right) spectra at the

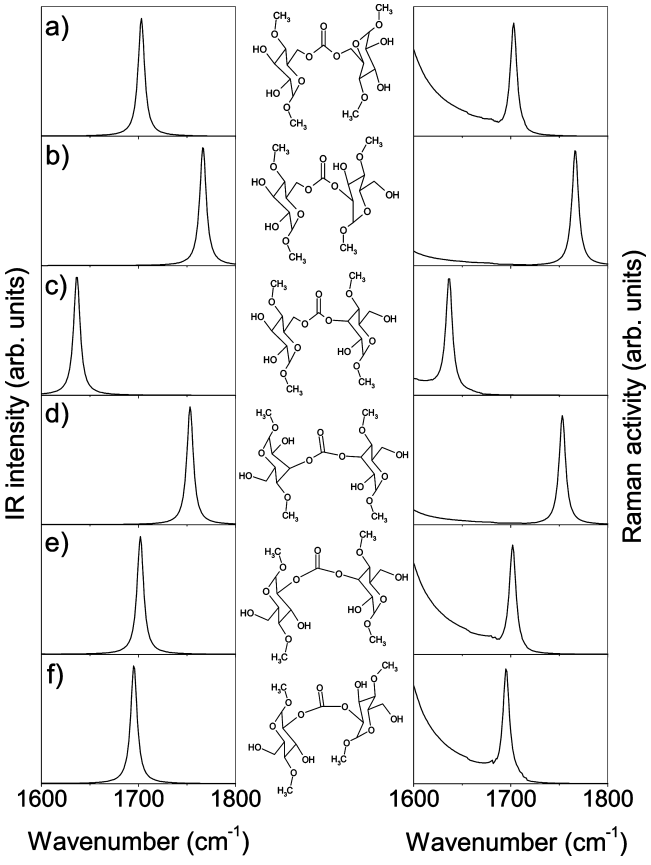

Figure 4. Computed IR (left panel) and Raman (right panel) spectrum of carbonate functional group for the model structures **1**–**6** (a–f) in the wavenumber range 1600–1800 cm^{-1}.

DFT-B3LYP 6-31g level of theory in the wavenumber region 1600–1800 cm^{-1} for structures **1**–**6** (Figure 3) are shown. The computation provides a single vibrational mode (IR and Raman active) in the reported spectral region for each structure.

The analysis of the vibrational parameters clearly indicates that all computed normal modes falling in the wavenumber range 1600–1800 cm^{-1} correspond to vibrations mainly localized on the C=O groups belonging to the different regioisomeric carbonates. In Figure 5a–f, we report the

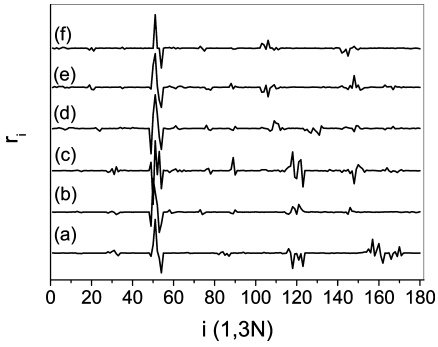

Figure 5. Normalized displacements r_i as a function of the atomic degree of freedom *i* for each atom of compounds **1**–**6** under the effect of the normal modes at 1703 cm^{-1} for structure **1** (a), 1766 cm^{-1} for structure **2** (b), 1636 cm^{-1} for structure **3** (c), 1753 cm^{-1} for structure **4** (d), 1701 cm^{-1} for structure **5** (e), and 1695 cm^{-1} for structure **6** (f).

normalized displacements r_i (i = 1, 3*N* where *N* is the number of the atoms for the structures **1**–**6**) for each atom under the effect of the normal modes obtained at 1703 cm^{-1} for structure **1** (a), 1766 cm^{-1} for structure **2** (b), 1636 cm^{-1} for structure **3** (c), 1753 cm^{-1} for structure **4** (d), 1701 cm^{-1} for structure **5** (e), and 1695 cm^{-1} for structure **6** (f). Using this representation of the eigenvectors, we can visualize the Cartesian displacements $r_1 = X_1$, $r_2 = Y_1$, $r_3 = Z_1$, $r_4 = X_2$,... for each atom due to the action of the corresponding normal mode. The labels for C and O atoms of the carbonyl group are 17 and 18, respectively, corresponding to i = 49–54 in the x axis of Figure 5. (The full list of the atom numbers is given in the Supporting Information.) As it clearly appears from an inspection of the Figure, the form of the eigenvectors corresponding to these normal modes suggests that in all cases the vibration can be assigned to the C=O stretching.

The data point out that C=O stretching frequency depends markedly on two factors: (i) the type of CD hydroxyl groups involved in the ester bond, that is, primary or secondary OH groups, and (ii) the position of the secondary OH group in the glucose frame, that is, OH(2) versus OH(3). Moreover, the calculated frequencies allow us to rule out structures **3** and **6** due to the fact that the calculated frequencies are too low (1636 (structure **3**) and 1695 cm^{-1} (structure **6**)) and do not match the experimental values. Conversely, the difference of the calculated wavenumber positions and the experimental values for the stretching vibration of C=O group of **1**, **2**, **4** and **5** is not sufficiently large for a clear-cut rebuttal of any of these models. In this stage, the two ω_{CO1} and ω_{CO2}, experimental components can be, in principle, assigned to four different computed modes (structures **1**, **2**, **4**, and **5**). The unambiguous assignment of ω_{CO1} and ω_{CO2}, requires additional structural information. We used the analysis of the IR spectral region between 3000 and 3700 cm^{-1}, where the OH stretching vibrations fall. This spectral window is particularly informative on the change of the bond strength and the relative populations of the different types of O–H groups present in the system. By following an approach successfully applied for pure β-CD and its inclusion complexes,[36–40] the different vibrational components contributing to the total O–H stretching band can be

dx.doi.org/10.1021/jp307978e | J. Phys. Chem. B 2012, 116, 13133–13140

recognized in the FTIR-ATR spectra in the wavenumber range 3000−3700 cm^{-1}.

In particular, Fourier self-deconvolution and band fitting procedures[41,42] allowed us to identify five sub-bands assigned to the OH stretching vibrations of primary and secondary OH groups of β-CD and of OH groups belonging to interstitial and intracavity H2O molecules.[43,44]

Figure 5a shows the experimental FTIR-ATR spectra of β-CDCDI1*n* (where *n* = 2, 3, 5, and 8) acquired at *T* = 300 K in the wavenumber range 3000−3700 cm^{-1}. Typical examples of best-fitting results for β-CDCDI12 and β-CDCDI18 are reported in Figure 6b,c, respectively.

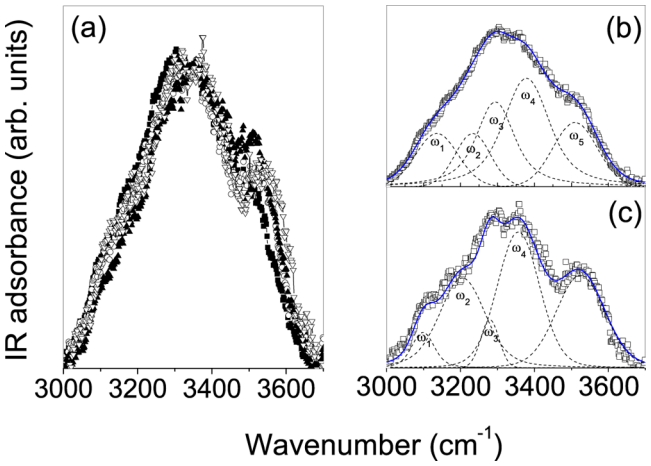

Figure 6. (a) Experimental FTIR-ATR spectra for β-CDCDI12 (■), β-CDCDI13 (○), β-CDCDI15 (▲), and β-CDCDI18 (▽) at *T* = 300 K in the wavenumber range 3000−3700 cm^{-1}. (b,c) Typical example of best-fitting results for β-CDCDI12 and β-CDCDI18, respectively, at *T* = 300 K.

As in the case of the C═O stretching vibration, the accurate curve-fitting analysis of the O−H stretching band as a sum of individual components was supported by the calculation of the second derivative of the IR spectra (data not reported here). The presence of five subminima in the second-derivative diagram suggested the use of five sub-bands for the description of the existing types of OH oscillators. These bands are centered at $\omega_1 \approx 3100$ cm^{-1}, $\omega_2 \approx 3190$ cm^{-1}, $\omega_3 \approx 3270$ cm^{-1}, $\omega_4 \approx 3360$ cm^{-1}, and $\omega_5 \approx 3520$ cm^{-1}. According to previous studies,[45] ω_1 and ω_3 are assigned to stretching vibrations of OH groups of water molecules localized in the interstices among different β-CD units, whereas ω_5 is assigned to the OH stretching of water molecules placed in the hydrophobic cavity of β-CD. Similarly, the bands referred to as ω_2 and ω_4 are assigned to the stretching vibrations of secondary and primary OH groups of β-CD, respectively. The corresponding main fit parameters, that is, peak wavenumber (ω_i, cm^{-1}) and percentage intensity (I_i, %), along with the vibrational assignment of the observed sub-bands for the O−H stretching region, are reported in Table 1 for β-CDCDI1*n* (where *n* = 2, 3, 5, and 8) at different temperatures.

The comparison of the percentage intensities of the bands assigned to the stretching vibrations of secondary and primary OH groups of CD (I_2 and I_4, respectively) is reported in Figure 7 as a function of the β-CD/CDI molar ratio and at *T* = 300 K. As is well known, the percentage intensities of IR bands are proportional to the populations of the oscillators involved in the corresponding vibration, so, in this case, to the populations of the two different types of OH groups assigned to each component.

We notice that whereas, on one side, the I_2 values (stretching vibration of secondary OH groups, open circles in Figure 6) remain substantially unchanged, the I_4 values (stretching vibration of primary OH groups, open down triangles in Figure 6) decrease by ∼7.4% with increasing molar ratio *n*. This trend indicates a major involvement of the primary OH groups in the chemical derivatization of CD during the cross-linking reaction compared with the secondary OH. This finding leads us to rule out structures **4** and **5** (see Figure 3) in which the carbonate group connects two glucose units via secondary OH on each. In this stage, among the six model dimers hypothesized in Figure 3, only structure **1** and **2** provide good matching between experimental and calculated vibrational profiles in both of the analyzed regions. On this basis, the assignment of the experimental spectral components ω_{CO1} and ω_{CO2} to the computed modes at 1703 (structure **1**) and at 1766 cm^{-1} (structure **2**), respectively, can be confidently proposed. It is worth noting that ω_{CO1} and ω_{CO2} correspond to the carbonyl stretching of carbonate groups formed by two primary and by one primary and one secondary OH group, respectively.

The total estimated intensity for the C═O stretching band (I_{CO1} + I_{CO2}) and its spectral components I_{CO1} and I_{CO2}, observed in the FTIR-ATR and Raman spectra of nanosponges, is reported in Figure 8a,b, respectively, as a function of molar ratio *n*. To attempt a quantitative analysis, the spectra were preliminarily normalized to the intensity of the bands at ∼1015 and 2903 cm^{-1} for IR and Raman data, respectively. These vibrational modes were assumed to be reliable internal standard because they are, respectively, related to the stretching vibrations of C−O and CH_2 groups of the cyclodextrin units not involved in polymerization with CDI.

The normalized intensities I_{CO1} and I_{CO2} reflect the population of the corresponding species, that is, the amount of the two type of carbonyls present in the polymeric network. A significant increase in the number of oscillators ω_{CO1} is found at high values of *n*, as can be observed by both IR and Raman data of Figure 8a,b, respectively. On the contrary, the intensity I_{CO2} does not show appreciable variations with increasing *n*. These trends suggest that the ester groups involving the primary OH groups of CD are prevalent with respect to those connecting the secondary OHs, in agreement with the results extracted by the analysis of the high-frequency region.

At high values of molar ratio, *n*, the excess of bonds involving primary OH groups of CD appears even more evident, as shown in the insets of Figure 8a,b, where the I_{CO2}/I_{CO1} ratio is reported as a function of *n*.

It is also worth mentioning that good agreement is found when comparing IR and Raman results summarized in Figure 8a,b, thus confirming the reliability of the data treatment and normalization procedure. The total intensity I_{CO1} + I_{CO2} of the C═O stretching band reflects the total number of the carbonyls groups present in the polymer, which is, in turn, directly proportional to the degree of cross-linking of the nanosponges network. As can be observed in Figure 8a,b, the plots show an increase in the reticulation of the systems for molar ratios *n* > 2.

Interestingly, increasing the number of cross-linkers in CDI-nanosponges does not generate a corresponding increase in the stiffness of the polymer, as suggested by the comparison of the present data with the results of some low-frequency Raman and Brillouin scattering experiments recently published.[26] In those

dx.doi.org/10.1021/jp307978e | J. Phys. Chem. B 2012, 116, 13133−13140

Table 1. Main Best-Fit Parameters, That Is, Wavenumbers ω_i (i = 1, 2, 3, 4, 5) (cm^{-1}), Percentage Intensities I_i (i = 1, 2, 3, 4, 5) (%), and Vibrational Assignment of the Observed Sub-Bands for the O−H Stretching Region of β-CDCDI Nanosponges at the Analyzed CDI/β-CD Molar Ratios

	O−H stretching intersititial H_2O		O−H stretching secondary OH groups		O−H stretching interstitial H_2O		O−H stretching primary OH groups		O−H stretching intracavity H_2O	
T (K)	ω_1 (cm^{-1})	I_1 %	ω_2 (cm^{-1})	I_2 %	ω_3 (cm^{-1})	I_3 %	ω_4 (cm^{-1})	I_4 %	ω_5 (cm^{-1})	I_5 %
					β-CDCDI12					
250	3119.1	13.1	3212.2	14.3	3288.0	19.4	3384.2	32.6	3525.2	20.6
260	3097.7	9.5	3192.6	16.5	3277.0	19.1	3370.3	33.2	3514.8	21.7
270	3093.5	6.5	3168.3	18.0	3252.6	14.3	3350.2	38.2	3503.8	23.0
280	3098.3	4.6	3175.2	18.3	3255.1	10.6	3348.0	42.6	3511.5	23.9
290	3096.5	4.3	3175.1	20.6	3254.6	9.0	3341.7	42.1	3499.8	24.0
300	3097.2	4.2	3176.6	21.8	3256.2	8.6	3344.7	42.4	3504.5	23.0
310	3097.7	4.2	3192.3	21.6	3270.3	8.7	3358.8	42.7	3518.5	23.8
320	3097.2	4.1	3175.7	21.1	3256.2	8.6	3344.7	42.4	3499.7	23.8
					β-CDCDI13					
300	3093.8	4.3	3177.6	22.0	3257.4	8.5	3352.7	41.0	3525.1	24.2
					β-CDCDI15					
250	3104.2	10.8	3203.0	16.2	3290.0	17.9	3378.1	30.7	3526.5	24.4
260	3098.0	9.2	3183.7	17.0	3268.0	16.7	3357.6	31.5	3506.2	25.6
270	3104.2	6.6	3194.1	16.6	3269.8	9.6	3346.6	35.4	3500.7	31.8
280	3093.4	6.1	3197.5	20.6	3263.8	9.1	3353.7	36.2	3516.1	28.0
290	3096.8	4.6	3202.7	21.2	3277.5	6.7	3365.4	37.5	3521.4	30.0
300	3101.1	4.5	3209.7	22.2	3276.3	5.9	3366.0	37.3	3515.9	30.1
310	3088.5	4.1	3205.5	22.8	3281.0	5.3	3361.1	37.5	3514.4	30.3
320	3088.5	4.5	3204.2	22.8	3281.0	5.1	3362.1	37.9	3515.6	29.8
					β-CDCDI18					
250	3085.6	11.0	3193.3	14.1	3279.1	14.2	3374.4	28.9	3537.5	31.8
260	3100.8	8.8	3183.8	17.3	3269.8	11.6	3365.1	30.3	3537.2	32.0
270	3108.0	6.7	3197.3	18.7	3269.4	6.4	3360.6	35.0	3537.7	33.2
280	3090.0	6.1	3185.6	20.7	3267.9	5.5	3352.7	35.6	3529.7	32.1
290	3097.7	5.6	3193.1	21.3	3266.7	5.4	3351.5	35.6	3526.7	32.1
300	3098.4	5.4	3204.8	24.0	3279.1	5.2	3356.4	35.0	3524.2	31.5
310	3098.2	4.5	3201.6	24.2	3274.8	3.1	3361.5	35.5	3524.6	32.7
320	3099.1	4.5	3202.4	24.3	3275.1	3.0	3362.3	36.1	3527.3	32.1

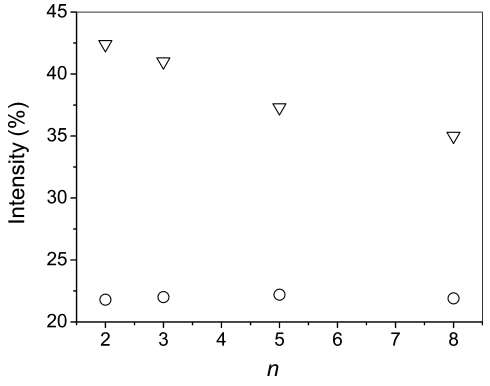

Figure 7. Percentage intensities of the different spectral contributions to the OH stretching band at 300 K for β-CDCDI nanosponges as a function of β-CD:CDI molar ratio n. I_2: open circles, I_4: open down triangles.

experiments, the observed shifts of the frequency position of Boson and Brillouin peaks are directly connected to the stiffness of the system over a length scale ranging from a few to hundreds of nanometers. The frequency position of the Boson and Brillouin peaks shows a slight decrease with increasing the amount of cross-linker with respect to β-CD within the explored CDI/βCD molar ratios. Therefore, the combined use of IR/Raman spectroscopies and inelastic light scattering experiments (low-frequency Raman and Brillouin spectroscopy) provides a powerful investigating task for correlating the molecular structure with the mechanical properties of cross-linked polymers.

As final point, the effect of temperature was studied. The deconvolution procedure was applied to the OH stretching band observed in the FTIR-ATR spectra of the investigated nanosponges at different values of temperature, in the 250−320 K range. The purpose of this analysis was probing the nature and the extent of changes in the hydrogen bond network of the polymers as a function of temperature. The best-fitted FTIR-ATR spectra and the deconvoluted components in the 3000−3700 cm^{-1} region for β-CDCDI15 at T = 250, 290, and 320 K are shown in Figure 9a−c, as an example.

The percentage intensities I_i (i = 1, 2, 3, 4, 5) of the different spectral contributions to the O−H stretching band are reported as a function of temperature in Figure 10a−c for β-CDCDI12, β-CDCDI15, and β-CDCDI18, respectively.

As it appears clear from an inspection of Figure 10, increasing T causes a decrease in I_1 and I_3 and an increase in I_2, I_4 and I_5. This trend indicates a temperature-induced destructuring effect on the hydrogen-bonded network of the nanosponge, resulting, on one side, in the diminishing of the number of interstitial water molecules linked to cyclodextrins and, on the other side, in the increase in the populations of secondary and primary OH groups as well as of intracavity water in molecular form.

dx.doi.org/10.1021/jp307978e | J. Phys. Chem. B 2012, 116, 13133−13140

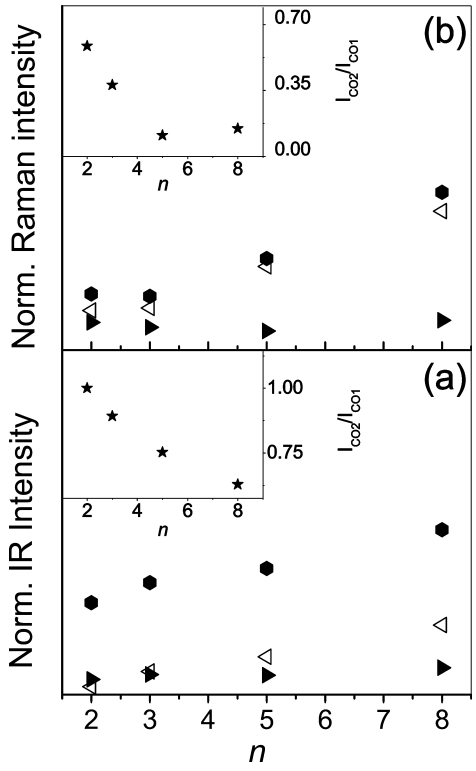

Figure 8. Normalized intensity of the C═O stretching band (closed hexagons) and its different spectral components I_{CO1} (open left triangles) and I_{CO2} (closed right triangles) observed in FTIR-ATR (a) and Raman (b) spectra as a function of n. Inset: I_{CO2}/I_{CO1} ratios observed in FTIR-ATR (a) and Raman (b) spectra as a function of n.

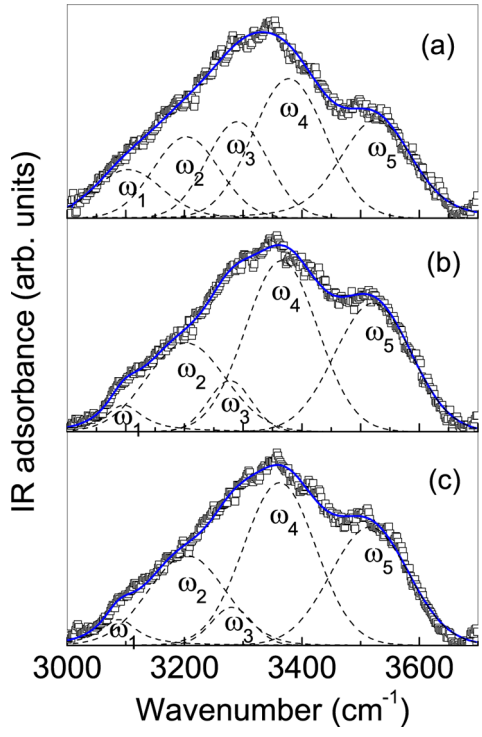

Figure 9. Experimental FTIR-ATR spectra for β-CDCDI15 at 250 (a), 290 (b) and 320 K (c), together with the best-fit (continuous blue line) and the deconvolution components (dashed lines).

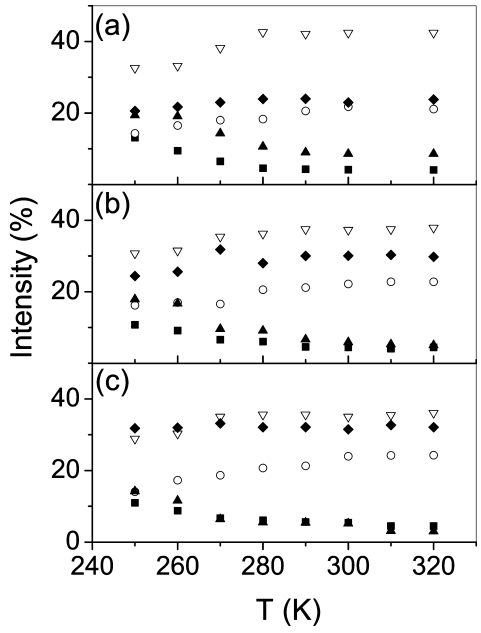

Figure 10. Temperature evolution of the percentage intensities I_i (i = 1, 2, 3, 4, 5) of the different contributions to the O−H stretching band for β-CDCDI12 (a), β-CDCDI15 (b), and β-CDCDI18 (c). I_1: ■, I_2: ○, I_3: ▲, I_4: ▽, I_5: ◆.

CONCLUSIONS

The vibrational dynamics of a new class of cycodextrin-based polymers was here explored to provide information on the molecular structures of β-CDNS as increasing the β-CD/CDI molar ratios. The simultaneous analysis of different spectral ranges (1650−1800 and 3000−3700 cm^{-1}) in both the FTIR-ATR and Raman spectra allowed us to develop a reliable strategy for quantifying the number of the C═O functional groups present in the polymeric network, in turn related to the cross-linking degree of the system. For this aim, best-fitting procedures were used for the quantitative analysis of the vibrational spectra. The assignment of the experimental bands and the interpretation of the data were supported by quantum chemical computations performed on the model structures of the six different carbonates, which can be formed during the synthesis of CDI-nanosponges. The comparison between experimental and simulation results revealed a major involvement of the primary OH groups of cyclodextrin units during the cross-linking reaction compared with the secondary OHs. Finally, the detailed inspection of the high-frequency vibrational dynamics of nanosponges indicated a clear dependence from temperature of the H-bond network involving the OH groups of the molecule.

These results corroborate the validity of the experimental−numerical approach, recently successfully applied to the PMA-nanosponges case,[27] as a powerful tool to investigate amorphous polymeric systems for which the use of diffraction techniques is seriously hampered by the low or absent level of crystallinity.

ASSOCIATED CONTENT

Supporting Information

DFT-minimized structures of the six possible regioisomeric carbonates of model methyl-α-D-4-O-methylglucoside with the numbering of atoms used for the representation of eigenvectors

dx.doi.org/10.1021/jp307978e | J. Phys. Chem. B 2012, 116, 13133−13140

in Figure 4. This material is available free of charge via the Internet at http://pubs.acs.org.

AUTHOR INFORMATION

Corresponding Author

*E-mail: rossi@science.unitn.it.

Notes

The authors declare no competing financial interest.

ACKNOWLEDGMENTS

We thank Dr. A. Defant for useful discussions. B.R. acknowledges the financial support of the Regione Veneto, being the beneficiary of a scholarship within the Programma Operativo Regionale FSE 2007-2013.

REFERENCES

(1) Bender, M. L.; Komiyama, M. *Cyclodextrin Chemistry*; Springer, New York, 1978.
(2) Uekama, K.; Hirayama, F.; Irie, T. *Chem. Rev.* **1998**, *98*, 2045.
(3) Li, S.; Purdy, W. C. *Chem. Rev.* **1992**, *92*, 1457.
(4) Szejtli, J. *Chem. Rev.* **1998**, *98*, 1743.
(5) *Cyclodextrin Technology*; Szejtli, J., Ed.; Kluwer Academic Publishers: Boston, 1988.
(6) Szejtli, J.; Osa, T. *Comprehensive Supramolecular Chemistry (CDs)*; Pergamon: Oxford, U.K., 1996.
(7) *New Trends in Cyclodextrins and Derivatives*; Duchene, D., Ed.; Editions de Santè: Paris, 1991.
(8) Harata, K. *Trends Phys. Chem.* **1990**, *1*, 45.
(9) Amajjahe, S.; Choi, S.; Muntenau, M.; Ritter, H. *Angew. Chem., Int. Ed.* **2008**, *47*, 3435.
(10) Takashima, T.; Osaki, M.; Harada, A. *J. Am. Chem. Soc.* **2004**, *126*, 13588.
(11) Van de Manakker, F.; Vermonden, T.; Van Nostrum, C. F.; Hennink, W. E. *Biomacromolecules* **2009**, *10*, 3157−3175.
(12) Trotta, F.; Tumiatti, W. Cross-Linked Polymers Based on Cyclodextrin for Removing Polluting Agents. WO Patent 03/085002, 2007.
(13) Mhlanga, S. D.; Mamba, B. B.; Krause, R. W.; Malefetse, T. J. *J. Chem. Technol. Biotechnol.* **2007**, *82*, 382−388.
(14) Salipira, K. L.; Mamba, B. B.; Krause, R. W.; Malefetse, T. J.; Durbach, S. H. *Water SA* **2008**, *34*, 113−118.
(15) Arkas, M.; Allabashi, R.; Tsiourvas, D; Mattausch, E. M.; Perfler, R. *Environ. Sci. Technol.* **2006**, *40*, 2771−2777.
(16) Mamba, B. B.; Krause, R. W.; Malefetse, T. J.; Gericke, G.; Sithole, S. P. *Water SA* **2008**, *34*, 657.
(17) Alongi, J.; Poskovic, M.; Visakh, P. M.; Frache, A.; Malucelli, G. *Carbohydr. Polym.* **2012**, *88* (4), 1387.
(18) Enescu, D.; Alongi, J.; Frache, A. *J. Appl. Polym. Sci.* **2012**, *123* (6), 3545.
(19) Cavalli, R.; Trotta, R.; Tumiatti, W. *J. Inclusion Phenom. Macrocyclic Chem.* **2006**, *56*, 209−213.
(20) Swaminathan, S.; Pastero, L.; Serpe, L.; Trotta, F.; Vavia, P. R.; Aquilano, D.; Trotta, M.; Zara, G.; Cavalli, R. *Eur. J. Pharm. Biopharm.* **2010**, *74*, 193−201.
(21) Ansari, K. A.; Vavia, P. R.; Trotta, F.; Cavalli, R. *AAPS PharmSciTech* **2011**, *12*, 279−286.
(22) Trotta, F.; Tumiatti, W.; Cavalli, R.; Roggero, C. M.; Mognetti, B.; Berta Nicolao, G. Cyclodextrin-Based Nanosponges As a Vehicle for Antitumoral Drugs. WO Patent 09/003656, 2009
(23) Seglie, L.; Martina, K.; Devecchi, M.; Roggero, C.; Trotta, F.; Scariot, V. *Postharvest Biol. Technol.*. **2011**, *59*, 200−205.
(24) Vyas, A.; Shailendra, S.; Swarnlata, S. *J. Inclusion Phenom. Macrocyclic Chem.* **2008**, *62*, 23.
(25) Mele, A.; Castiglione, F.; Malpezzi, L.; Ganazzoli, F.; Raffaini, G.; Trotta, F.; Rossi, B.; Fontana, A. *J. Inclusion Phenom. Macrocyclic Chem.* **2011**, *69*, 403−409.
(26) Rossi, B.; Caponi, S.; Castiglione, F.; Corezzi, S.; Fontana, A.; Giarola, M.; Mariotto, G.; Mele, A.; Petrillo, C.; Trotta, F.; Viliani, G. *J. Phys. Chem. B* **2012**, *116* (17), 5323−5327.
(27) Castiglione, F.; Crupi, V.; Majolino, D.; Mele, A.; Rossi, B.; Trotta, F.; Venuti, V. *J. Phys. Chem. B* **2012**, *116* (27), 7952−7958.
(28) Castiglione, F.; Crupi, V.; Majolino, D.; Mele, A.; Panzeri, W.; Rossi, B.; Trotta, F.; Venuti, V. *J. Inclusion Phenom. Macrocyclic Chem.*, **2012**, in press. DOI: 10.1007/s10847-012-0106-z.
(29) Gajewski, J. J.; Gilbert, K. E. *PCModel 8.0. Molecular Modelling Software for Personal Workstation*; Serena Software: Bloomington, IN, 1993.
(30) Frisch, M. J.; Trucks, G. W.; Schlegel, H. B.; Scuseria, G. E.; Robb, M. A.; Cheeseman, J. R.; Montgomery, J. A., Jr.; Vreven, T.; Kudin, K. N.; Burant, J. C.; et al. *Gaussian 03*, revision C.02; Gaussian, Inc.: Wallingford, CT, 2004.
(31) Lee, C.; Yang, W.; Parr, R. G. *Phys. Rev. B* **1988**, *37*, 785.
(32) Becke, A. D. *J. Chem. Phys.* **1993**, *98*, 5648.
(33) Hariharan, P. C.; Pople, J. A. *Theor. Chim. Acta* **1973**, *28*, 213.
(34) Crupi, V.; Guella, G.; Majolino, D.; Mancini, I.; Paciaroni, A.; Rossi, B.; Venuti, V.; Verrocchio, P.; Viliani, G. *Philos. Mag.* **2011**, *91*, 1776−1785.
(35) Guella, G.; Mancini, I.; Mariotto, G.; Rossi, B.; Viliani, G. *Phys. Chem. Chem. Phys.* **2009**, *11*, 2420−2427.
(36) Crupi, V.; Ficarra, R.; Guardo, M.; Majolino, D.; Stancanelli, R.; Venuti, V. *J. Pharm. Biomed. Anal.* **2007**, *44*, 110−117.
(37) Cannavà, C.; Crupi, V.; Ficarra, P.; Guardo, M.; Majolino, D.; Stancanelli, R.; Venuti, V. *Vibr. Spectrosc.* **2008**, *48*, 172−178.
(38) Stancanelli, R.; Ficarra, R.; Cannavà, C.; Guardo, M.; Calabrò, M. L.; Ficarra, P.; Ottanà, R.; Maccari, R.; Crupi, V.; Majolino, D.; Venuti, V. *J. Pharm. Biomed. Anal.* **2008**, *47*, 704−709.
(39) Cannavà, C.; Crupi, V.; Ficarra, P.; Guardo, M.; Majolino, D.; Mazzaglia, A.; Stancanelli, R.; Venuti, V. *J. Pharm. Biomed. Anal.* **2010**, *51*, 1064−1068.
(40) Stancanelli, R.; Crupi, V.; De Luca, L.; Ficarra, P.; Ficarra, R.; Gitto, R.; Guardo, M.; Iraci, N.; Majolino, D.; Tommasini, S.; Venuti, V. *Bioorg. Med. Chem.* **2008**, *16*, 8706−8712.
(41) Pierce, J. A.; Jackson, R. S.; Van Every, K. W.; Griffiths, P. R.; Gao, H. *Anal. Chem.* **1990**, *62*, 477−484.
(42) Lórenz-Fonfria, V. A.; Padros, E. *Spectrochim. Acta, Part A* **2004**, *60*, 2703−2710.
(43) Egyed, O. *Vibr. Spectrosc.* **1990**, *1*, 225−227.
(44) Egyed, O.; Weiszfeiler, V. *Vibr. Spectrosc.* **1994**, *7*, 73−77.
(45) Gavira, J. M.; Hernanz, A.; Bratu, I. *Vibr. Spectrosc.* **2003**, *32*, 137−146.